Supplemental Information

Regulation of planar growth by the *Arabidopsis* AGC protein kinase UNICORN

Balaji Enugutti[1], Charlotte Kirchhelle[1], Maxi Oelschner[1], Ramon A. Torres-Ruiz[2], Ivo Schliebner[3], Dario Leister[3] and Kay Schneitz[1*]

[1]Entwicklungsbiologie der Pflanzen, Wissenschaftszentrum Weihenstephan, Technische Universität München, 85354 Freising, Germany

[2]Lehrstuhl für Genetik, Wissenschaftszentrum Weihenstephan, Technische Universität München, 85354 Freising, Germany

[3]Lehrstuhl für Molekularbiologie der Pflanzen (Botanik), Department Biologie I, Biozentrum, Ludwig-Maximilians-Universität München, 82152 Planegg-Martinsried, Germany

Supplemental Figures

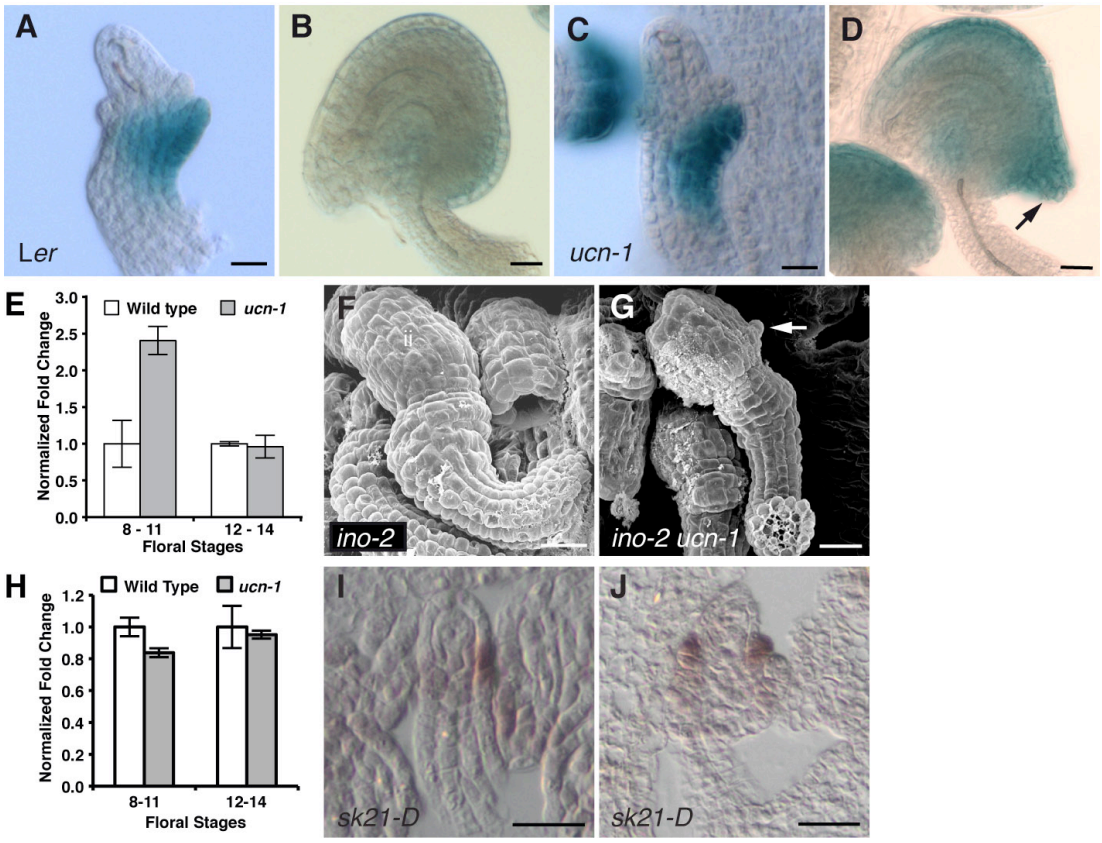

Fig. S1. Analysis of adaxial-abaxial polarity gene activity in *ucn* mutants. (*A-D*) Expression of the *pINO::GUS* reporter pRJM65 (1). (*A*) Stage 2-III wild-type ovule. Signal is detectable in the outer integument. (*B*) Stage 3-VI/4-I wild-type ovule. (*C*, *D*) *ucn-1*. Ovules of comparable stages as in (*A*, *B*) are depicted. The signal appears stronger in *ucn-1* ovules and is present in the protrusion (arrow). (*E*) qRT-PCR measurements of floral *INO* mRNA levels. Note the increased expression level of *INO* at floral stages 8-11. This indicates that *UCN* is a direct or indirect negative regulator of *INO* expression. Detectable *INO* expression at floral stages 12 to 14 further suggests that pRJM65 may lack some control elements for late *INO* expression (compare *B* with *E*). (*F*, *G*) SEMs of stage 4 ovules. (*F*) *ino-2* ovule. No outer integument. (*G*) *ino-2 ucn-1*. The inner integument still carries a protrusion (arrow).

This implies that *ucn-1* protrusions can occur in the absence of functional *INO*. (*H*) qRT-PCR measurements of floral *PHB* mRNA levels. The slightly decreased expression level of *PHB* in *ucn-1* at floral stages 8-11 is not significant (unpaired two-tailed t-test, Welch's correction, P=0.0715). (*I-J*) In situ hybridization on sectioned early *sk21-D* ovules using a *PHB* anti-sense probe (stage 2-I/II, stage 2-IV). No change compared to wild type (see Fig. 1*I, J*). Scale bars: (*A-D*) 30 μm, (*F*, *G, I, J*) 20 μm.

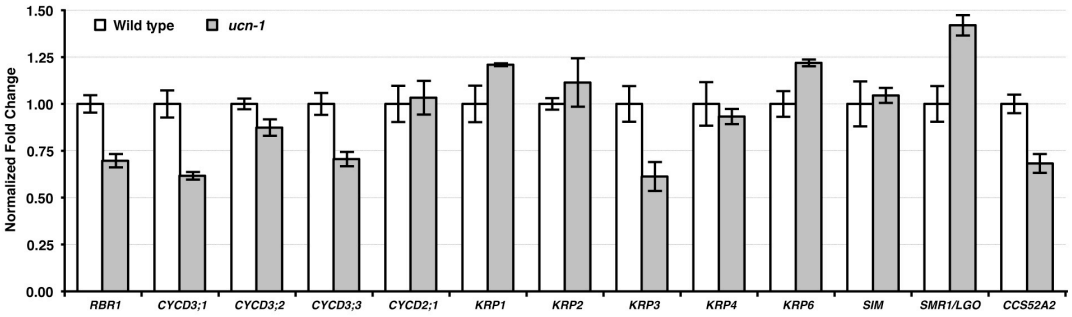

Fig. S2. Comparison of core cell cycle gene expression levels between wild-type and *ucn-1* petals by qRT-PCR. Petals from stage 10 to 12 flowers were used. Cell cycle genes were selected from (2).

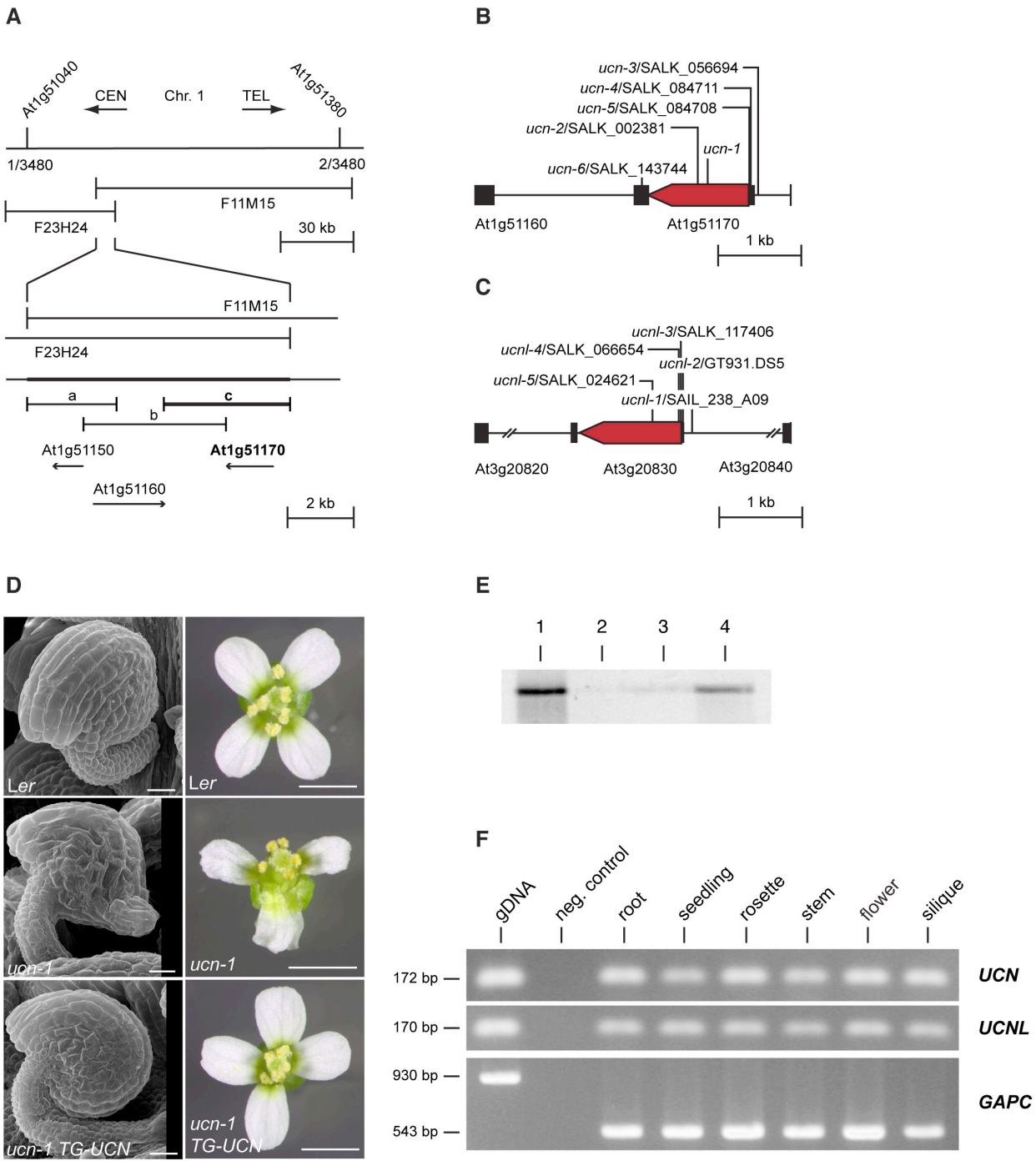

Fig. S3. Molecular characterization of *UCN* and *UCNL*. (*A*) Molecular identification of *UCN*. The upper panel represents the genomic interval between the two closest genetic markers. The recombination frequency for each marker is given. The extent of two genomic BAC clones is outlined as well. Both BAC clones could rescue the *ucn* phenotype. The lower panel focuses on the overlap of the two rescuing BAC clones

(indicated by the bold horizontal line). The three candidate genes within this region, and their orientation, are indicated by the extent and the orientation of the arrows. The a/b and c genomic clones used in further *ucn* rescue experiments are outlined. The c genomic clone, indicated by the bold horizontal line, rescued the *ucn* phenotype. (*B*) Genomic map of *UCN* highlighting the position of several T-DNA insertion sites. Black boxes mark the 5' and 3' UTRs, respectively. The arrow indicates the extent and the orientation of the open reading frame. In *ucn-2* the insertion results in a predicted shorter protein, which deviates beginning at L209 from the UCN sequence and carries an undetermined number of aberrant residues. (*C*) Genomic map of *UCNL* depicting the position of different T-DNA insertion sites. Black boxes mark 5' and 3' UTRs, respectively. The arrow indicates the extent and the orientation of the open reading frame. In *ucnl-3* the insertion results in a predicted three residues protein (M1-DA*) with the aspartate and the alanine being aberrant residues. In *ucnl-5* the insertion results in a predicted short protein at L116 followed by ten aberrant residues and a stop (L115-RILWCKQIDA*). In *ucnl-4* the insertion resides at S10 followed by an undermined number of aberrant residues. (*D*) Genomic rescue of *ucn-1*. Note that a *ucn-1* plant carrying a 3.8 kb genomic *UCN* DNA construct (*TG-UCN*) (c-construct described in (*A*)) shows apparently normal ovules and flowers. (*E*) In vitro chloroplast import assay. Radiolabelled UCN translated *in vitro* (lane 4; 10% of translation product) was incubated with isolated chloroplasts for 30 min at 25°C. Chloroplasts were recovered by centrifugation through 40% Percoll (lane 1). Thermolysin was added after termination of import reaction to remove adhererent preproteins (lane 2). As control, thermolysin was added to 10% of the translation product (lane 3). Results do not suggest import of UCN into chloroplasts. (*F*) Tissue distribution of *UCN* and *UCNL* expression as revealed by semi-quantitative reverse transcription PCR. The

result obtained after 26 cycles for all tested genes is shown. *GAPC* served as control (3). Root: 10-day seedling, seedling: 10-day seedlings, rosette leaves: 19-day plant, stem: 24-day plant, flowers: whole flowers from a 24-day plant, silique: all green siliques of a 24-day plant. In the negative control a template was omitted from the PCR-reaction. Abbreviations: Chr., chromosome; CEN, centromere; TEL, telomere. Scale bars in (*D*): left panel, 20 µm, right panel 0.5 mm.

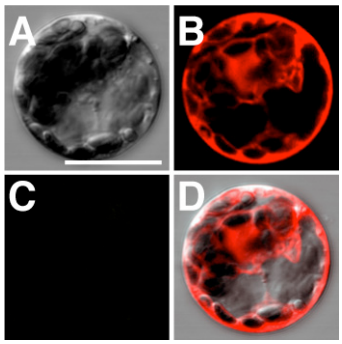

Fig. S4. BiFC control experiment. View of a typical protoplast from a batch co-transfected with 10 µg each of empty *pUC-SPYNE* and *pUC-SPYCE* plasmids. Four µg of plasmid *pGY-1:mCherry* (4) was used as transformation control. (*A*) Bright-field view. (*B*) Signal distribution of free mCherry (red signal). (*C*) YFP channel. Note the absence of detectable signal (10 biological replicates, > 1000 viable protoplasts scored). (*D*) Merge. Co-transfection of 4 µg each of *pSPYNE-UCN/pSPICE-UCN* plasmids results in detectable signal (Fig. 3*D*-*G*). Scale bar: 30 µm.

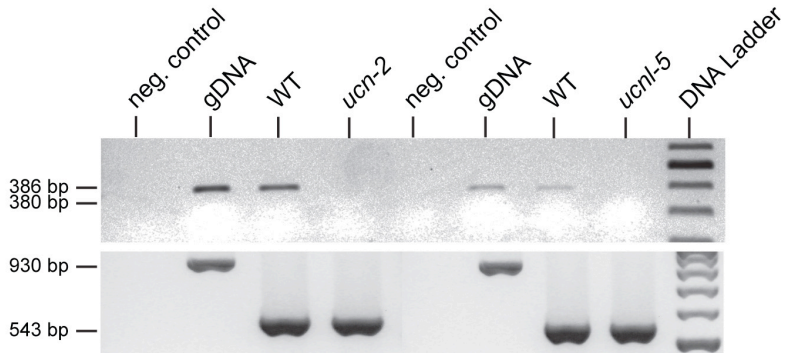

Fig. S5. Absence of *UCN* and *UCNL* wild-type transcripts in *ucn-2* and *ucnl-5* mutants. Results of an RT-PCR reaction (32 cycles) are shown. In the negative control a template was omitted from the PCR-reaction. Upper panel: Detection of *UCN* and *UCNL* transcripts. Left section: *UCN* (primers UCN (RT)_F/ UCN (RT)_R). Right section: *UCNL* (primers UCNL (RT)_F/ UCNL (RT)_R). Note that in both instances no wild-type transcript can be detected. Lower panel: control reactions using *GAPC* (3) as reference.

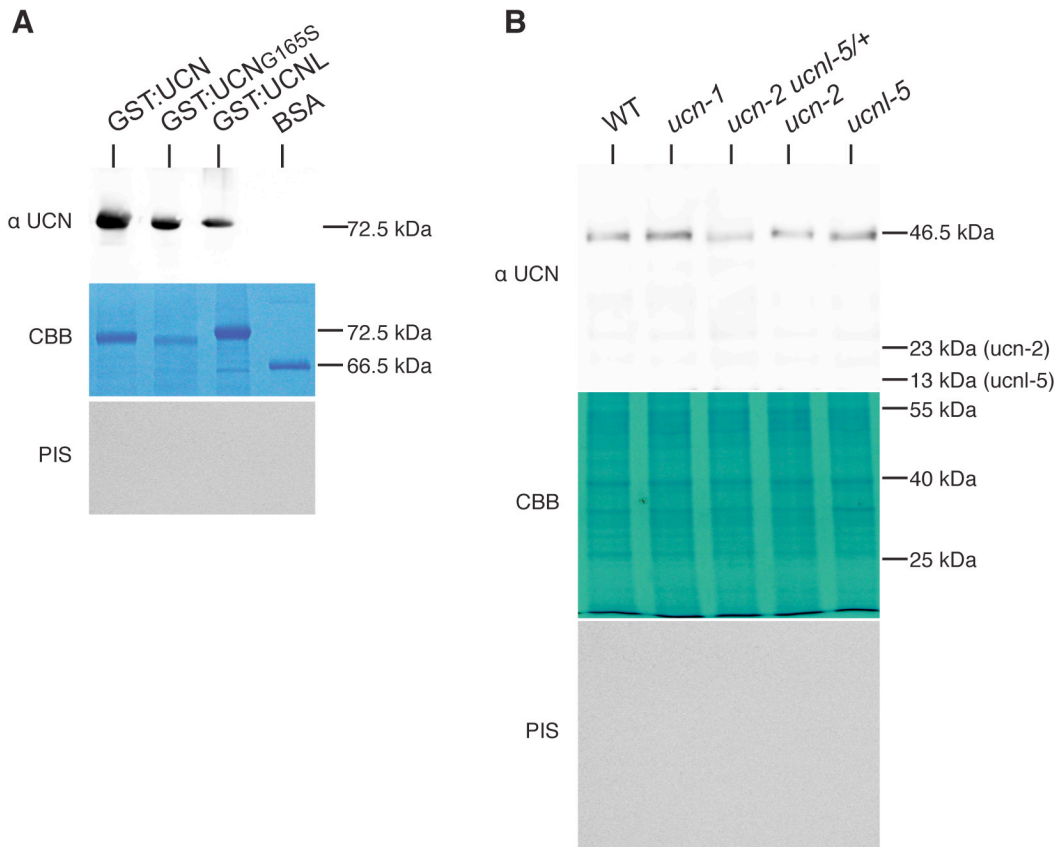

Fig. S6. The rabbit polyclonal anti-UCN antiserum recognizes UCN, UCN_{G165S} and UCNL. Upper panels show the anti-UCN antibody-specific chemiluminescence signals. Middle panels depict equivalent coomassie blue-stained protein gels. Bottom panels reveal the absence of signals when the protein blots were probed with pre-immune serum. (*A*) Detection of affinity-purified recombinant GST:UCN, $GST:UCN_{G165S}$ and GST:UCNL proteins. The antiserum recognizes GST:UCNL less efficiently than GST:UCN or $GST:UCN_{G165S}$. It does not detect BSA. (*B*) Visualization of UCN, UCN_{G165S} and UCNL proteins in root extracts from 12 day-old seedlings of the indicated genotypes. 40 μg total protein was loaded per lane. The predicted size of the mutant UCN and UCNL proteins are indicated to the right. Note that no signal at the expected size is detected in *ucn-2* and *ucnl-5* extracts indicating that the two mutants carry null-alleles. The approximately 40 kDa band in the coomassie blue gel conveniently serves as loading control. Abbreviations: BSA,

bovine serum albumin; CBB, coomassie brilliant blue gel; kDa, kilodalton; PIS, pre-immune serum; WT, wild type.

A

Genotype	Phenotype
ucn-2	WT
ucnl-5	WT
ucn-2 ; *ucnl-5/+*	WT
ucn-2 ; *ucnl-5*	lethal (100%)
ucn-1/+	WT
ucn-1	*ucn-1* (p. lethal)
ucn-1 ; *ucnl-5*	*ucn-1* (p. lethal)

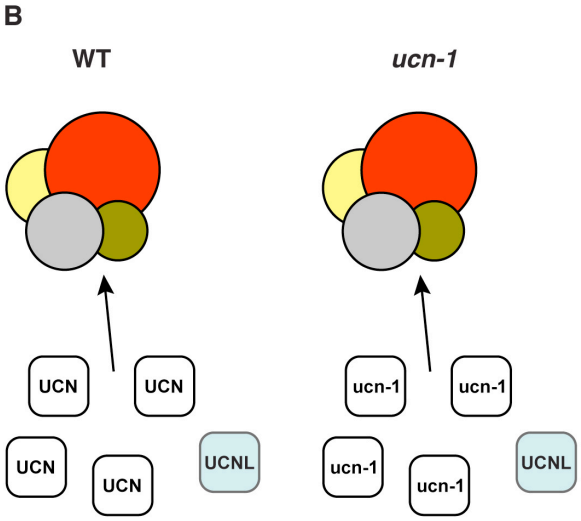

Fig. S7. Titration model explaining the *ucn-1* genetics. (*A*) A list of different genotypes and respective phenotypes. The T-DNA insertions in *ucn-2* and *ucnl-5* result in null alleles (no aberrant UCN or UCNL proteins detectable in root extracts, Fig. S5 and Fig. S6). The *ucn-2* and *ucn-2 ; ucnl5-/+* combinations appear wild-type. The *ucn-2 ucnl-5* double mutants exhibit full embryo lethality. These results reveal a requirement for *UCNL*. The *ucn-1* allele is strictly recessive (reciprocal crosses between L*er* and *ucn-1*; > 100 F1 plants scored). The *ucn-1* homozygotes exhibit partial lethality (25 percent) with similarly aberrant embryos as observed in *ucn-2 ucnl-5* (Fig. 2). This suggests that *ucn-1* is a hypomorph, at least with respect to embryo development. (*B*) A cartoon outlining how UCN and UCN_{G165S} may titrate UCNL in flowers. Left panel: In wild type, UCN protein is present at much higher levels compared to UCNL (hypothesis based on qRT-PCR results in Fig. 3C) and outcompetes UCNL in binding to a target protein complex. In addition, UCNL only

exhibits 72 percent amino acid identity with UCN. Therefore, UCNL may not be quite as active as UCN. Right panel: In *ucn-1* plants, the UCN_{G165S} (ucn-1) protein is still present at much higher levels than UCNL (inferred from Fig. 3C. In addition, there is no compensatory upregulation of *UCNL* transcription in *ucn-1* flowers). In addition, UCN_{G165S} is partially active (only partial embryo lethality of *ucn-1*). Therefore, in *ucn-1* homozygotes UCN_{G165S} may still outcompete UCNL. In addition, potential UCN_{G165S}/UCN complexes may still be functional. Thus, although wild-type copies of UCNL are present they do not come into play. In summary, in *ucn-1*/+, sufficient UCN activity is provided to allow development of wild-type plants and in *ucn-1* homozygotes the UCN_{G165S} protein titrates out UCNL.

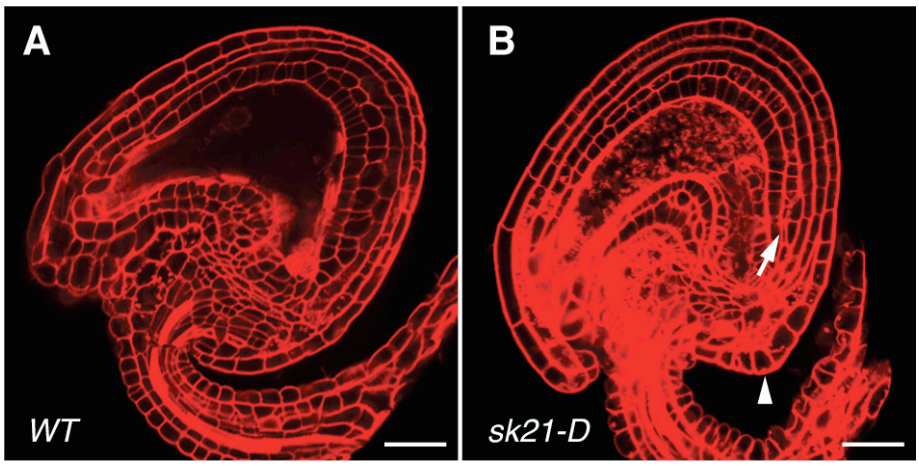

Fig. S8. Integument defects in the *sk21D* mutant. Confocal laser scanning micrographs of mature ovules after fertilization (about stage 4-V) stained with mPS-PI (5). (*A*) Wild-type. (*B*) *sk21-D*. Arrow indicates periclinal divisions. Note the *ucn*-like protrusion (arrowhead). Scale bars 20 µm.

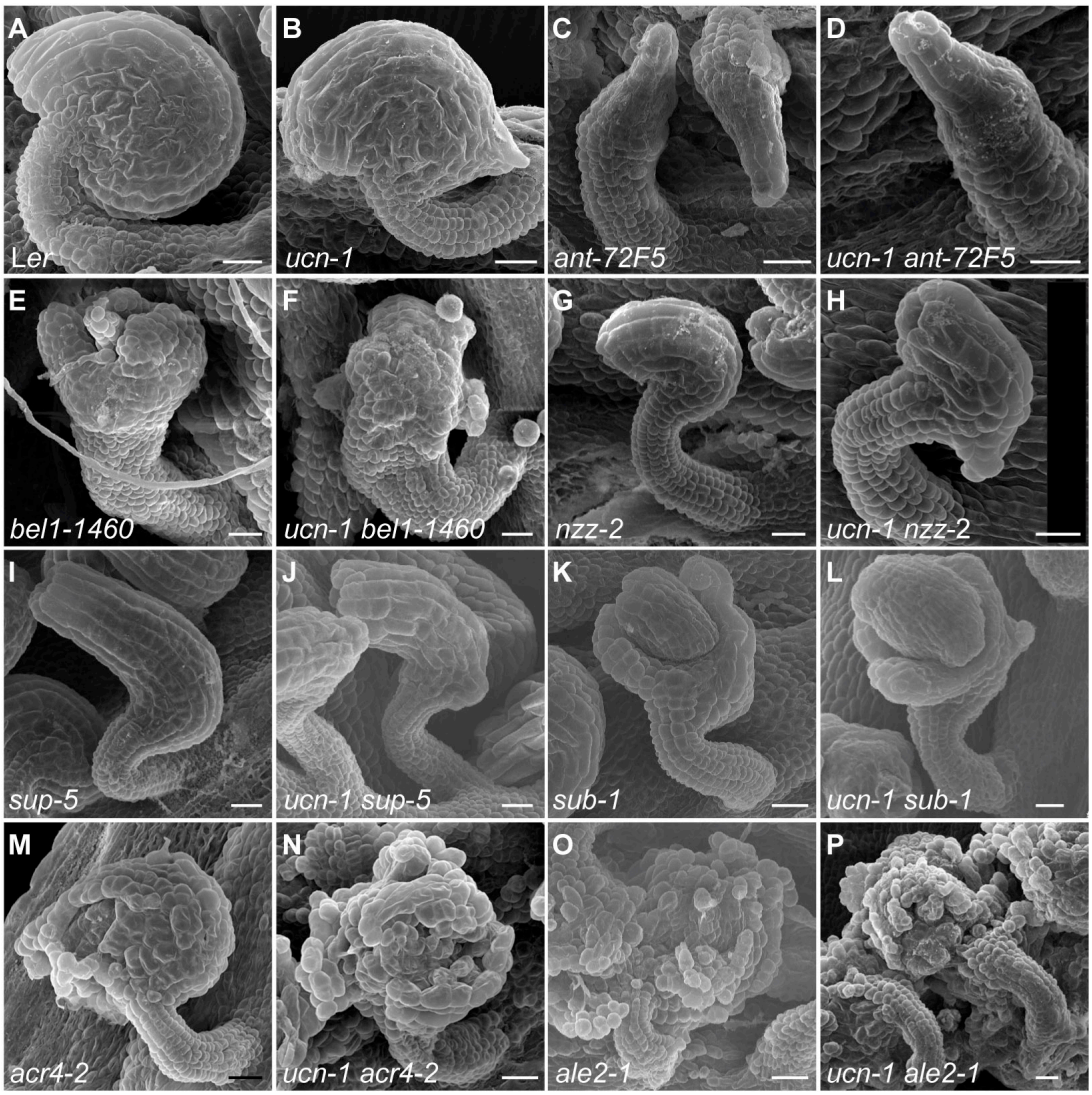

Fig. S9. Analysis of ovule phenotypes of various double mutants. Scanning electron micrographs of early stage 4 ovules are depicted. (*A*, *B*) Ler and *ucn-1* controls. (*C*, *D*) *ucn-1 ant-72F5* analysis. (*D*) Note the absence of integuments and epistasis of *ant-72F5*. As *ant* mutants fail to initiate integuments the result indicates that *ANT* acts prior to *UCN* in integument development. (*E*, *F*) *ucn-1 bel1-1460* analysis. (*E*) The *bel1* ovules are characterized by aberrant outgrowths in place of normal integuments. (*F*) Additive phenotype. Note the presence of *ucn-1* like protrusions on *bel1*-like outgrowths. (*G*, *H*) *ucn-1 nzz-2* analysis. (*H*) Additive phenotype. Note the occurrence of an *ucn-1*-like outgrowth on a *nzz-like* outer integument. (*I*, *J*) *ucn-1 sup-5* analysis.

(*J*) Additive phenotype. An *ucn-1*-like protrusion is seen on a *sup-5*-like outer integument. (*K*, *L*) *ucn-1 sub-1* analysis. (*L*) Additive phenotype. Note the presence of *ucn-1*-like protrusions on the *sub-1*-like outer integument. (*M*, *N*) *ucn-1 acr4-2* analysis. (*M*) There is aberrant integument development in *acr4-2* ovules, which includes the formation of protrusions. (*N*) Perhaps slightly more exaggerated integument development in *ucn-1 acr4-2* ovules suggested by an increased number of protrusions. (*O*, *P*) *ucn-1 ale2-1* analysis. *ucn-1 ale2-1* and *ucn-1 acr4-2* ovules share a very similar phenotype (compare *P* with *N*). Scale bars: 20 μm.

Supplemental Tables

Table S1. Classes of embryo phenotypes in *ucn-1* and *ucn-2 ucnl-5* double mutants.

Genotype	Embryos scored	Embryos with horizontal/oblique cell division planes in the proembryo	Embryos with delayed proliferation in the pro-embryo	No embryo
Wt	200	0	0	04
ucn-1-/-	750	125	24	31
ucn-2-/- ucnl-5 +/-	180	29	05	09

Table S2. Summary of *ucn and ucnl* alleles.

Allele	Mutagen	Mutation#	Amino acid change/transcript	Background	Reference
ucn-1	EMS	C>T, 44345	G165S	L*er*	this study Schneitz et. al. 1997
ucn-2	T-DNA SALK_002381	44218/LB	L209--*	Col	this study
ucn-3	T-DNA SALK_056694	44942/LB	RNA+	Col	this study
ucn-4	T-DNA SALK_084711	44881/LB	RNA+	Col	this study
ucn-5	T-DNA SALK_084708	44869/LB	RNA+	Col	this study
ucn-6	T-DNA SALK_143744	LB/43554	RNA+	Col	this study
ucn-7	EMS TILLING	G>A, 44713	S42F	Col *er-105*	this study
ucn-8	EMS TILLING	C>T, 44029	G270E	Col *er-105*	this study
ucn-9	EMS TILLING	C>T, 43880	D320N	Col *er-105*	this study
ucn-10	EMS TILLING	G>A, 44474	D122N	Col *er-105*	this study
ucnl-1	T-DNA SAIL_238_A09	46938/LB	RNA+	Col	this study

ucnl-2	T-DNA GT931.DS5	46818/LB	RNA+	L*er*	this study
ucnl-3	T-DNA SALK_117406	46808/LB	M1--*	Col	this study
ucnl-4	T-DNA SALK_066654	LB/46780	S10--*	Col	this study
ucnl-5	T-DNA SALK_024621	46465/LB	L116-- *	Col	this study

[#]the coordinates refer to the BAC (F23H24 and MOE17) sequence and relate to the ATG of *UCN* (At1g51170) - 44847 bp and UCNL(At3g20830) - 46813 bp.
--*indicates various aberrant sequences of residues followed by a stop.

Table S3. Chlorophyll fluorescence parameters measured from *ucn-1* and wild-type leaves.

	ucn-1	Col-0
Fv/Fm	0.83 ± 0.01	0.84 ± 0.00
Φ_{II}	0.68 ± 0.04	0.67 ± 0.02
1-qP	0.04 ± 0.02	0.05 ± 0.03
NPQ	0.23 ± 0.04	0.30 ± 0.03

Mean values for five plants (± SD) are shown. Results do not suggest a function for *UCN* in chloroplast biology.

Table S4. Quantification of *ucn*-like ovule phenotype in *ucn-1*, *sk21-D*, and *ucn-1 ats-3* double mutants.

Genotype	No. of Ovules analyzed	No. of Ovules with *ucn-1* like protrusions	Percentage of ovules with a protrusion
Wt	600	0	0
ucn-1	600	552	92
sk21-D	245	112	46
ats-3	600	0	0
ucn-1 ats-3	600	74	12

Table S5. Primers used in this study.

Primer name	**Sequence (5' to 3')**
UCN (gen KpnI)_F	ATATAGGTACCATAACATCATAAATTTGGAGTTATTCG
UCN (gen PstI)_R	ATATACTGCAGTGTGTGCATTACAGATT
At1g51160 (KpnI)_F	ATATAGGTACCGTTCTTGTTAAGTACTATGTTTACTCG
At1g51160 (PstI)_R	ATATACTGCAGTCCACGCGTGGGAGAAT
At1g51150 (KpnI)_F	ATATAGGTACCGAATTCAGGAAGCTGTT
At1g51150 (BamHI)_R	ATATAGGATCCTGCTTCCGTCGTCTCCG
UCN (T-DNA_gt)_F	CGTAATCATCAAGTACCATGC
UCN (T-DNA_gt)_R	GGAGTTATTCGAGATGCA
UCN (Till)_F	AGGGACACGAGGAGACATAAACGCAAC
UCN (Till)_R	CACGCGTGGATCAGAAATCAACAAAC
UCNL (T-DNA_gt)_F	CACCTCCGTTAACAAATCCCACC
UCNL (T-DNA_gt)_R	ACTTAATATCATTCTTAAAGTATCGCAAATTC
UCN (pGEX_XmaI)_F	ATGCATCCCGGGATGGAGACAAGACCATCATCATCATC
UCN (pGEX_NotI)_R	ATATATGCGGCCGCTCAGAAATCAACAAACGGATTGTTTTC
UCN (K55E)_F	CTTCTCCCTTTGCTTTAGAACTCGTCGACAAATC
UCN (K55E)_R	GATTTGTCGACGAGTTCTAAAGCAAAGGGAGAAG
UCN (KpnI)_F	ATAGGTACCATGGAGACAAGACCATCATCATCATC
UCN (HindIII)_R	ATAAAGCTTTCAGAAATCAACAAACG
ATS (pGEX_BamHI)_F	ATATATGGATCCATGATGATGTTAGAGTCAAG
ATS (pGEX XhoI)_R	ATCTATCTCGAGTTAGCACTTGAGAAGGG
UCN (BiFC_AscI)_F	ATAGATGGCGCGCCATGGAGACAAGACCATCATCATC
UCN (BiFC_Xma)_R	ATATATCCCGGGGAAATCAACAAACG
ATS (BiFC_AscI)_F	ATAGATGGCGCGCCATGATGATGTTAGAGTCAAGAA
ATS (BiFC_Xma)_R	ATATATCCCGGGGCACTTGAGAAGGGTTAAATCACT
ATSsense_831_F	TAATACGACTCACTATAGGG ATGATGATGTTAGAGTCAAGA
ATSsense_831_R	TTAGCACTTGAGAAGGGTTAA
ATSas_831_F	ATGATGATGTTAGAGTCAAGA
ATSas_831_R	TAATACGACTCACTATAGGGTTAGCACTTGAGAAGGGTTAA
UCN (sqRT)_F	TCTTCCTCGTCCACGACTCTG
UCN (sqRT)_R	GCTAAGAGTTTTGGGAGAAATGG
UCN (RT)_F	CTCTCGGAGTTTTAACGTACGAG
UCN (RT)_R	AGAACACTCGTGCGGTAACGGTAAC
UCNL (sqRT)_F	ATGGAGCCATCACCGTCG
UCNL (sqRT)_R	GGGACGAGCTTGACCGC
UCNL (RT)_F	GAGACGCCGTTCAAGGGTAAG
UCNL (RT)_R	CGTAAAAACGATCCGTTTATTGA
GAPC (RT)_F	CACTTGAAGGGTGGTGCCAAG
GAPC (RT)_R	CCTGTTGTCGCCAACGAAGTC
UBC21 (qRT)_F	TCCTCTTAACTGCGACTCAGG
UBC21 (qRT)_R	GCGAGGCGTGTATACATTTG

At4g33380 (qRT)_F	TGAAGGAGAGGAAGAGCCTGAGGAA
At4g33380 (qRT)_R	CCCCATCTCACTGCAGCACCAC
At2g28390 (qRT)_F	AGATTGCAGGGTACGCCTTGAGG
At2g28390 (qRT)_R	ACACGCATTCCACCTTCCGCG
At5g46630 (qRT)_F	CCAAATGGAATTTCAGGTGCCAATG
At5g46630 (qRT)_R	CAATGCGTACCTTGAGAAAACGAAC
UCN (qRT)_F	GCCGTGCAAGGTGGGAAATTC
UCN (qRT)_R	AAGCTAAGAGTTTTGGGAGAAATGGG
UCNL (qRT)_F	CCATCACCGTCGTCCCCACCAT
UCNL (qRT)_R	CGCCTTTACCGAGGATTTTGAGAGC
INO (qRT)_F	GCTCCCCAACATGACGACAACA
INO (qRT)_R	GCTTGTAAACGGTACACTCACCAGCA
ATS (qRT)_F	GGATCACCAGGAGAAGGAAAGGT
ATS (qRT)_R	GCACAGATGATGAGTTTGGCGA
RBR1 (qRT)_F	CGCCGTCAAGGGAGAATAGGG
RBR1 (qRT)_R	AGCAGCGGCTTTACGGCAGG
CYCD3;1 (qRT)_F	CCTCCTCTCTGTAATCTCCGATTCA
CYCD3;1 (qRT)_R	ATAATTCGCATCATGGTAGCTGC
CYCD3;2 (qRT)_F	TGTCTCAGCTTGTTGCTGTGGCT
CYCD3;2 (qRT)_R	TGCTTCTTCCACTTGGAGGTCT
CYCD3;3 (qRT)_F	ACTCAAAGTTGATTCGGAGAAGGT
CYCD3;3 (qRT)_R	GGACTAGCGGGTTGTTGCAT
CYCD2;1 (qRT)_F	GACAAGGATTGGGCTGCTCAGT
CYCD2;1 (qRT)_R	ACAAACTTGGGATCTTCCACCTGTA
KRP1 (qRT)_F	TCGTCGTCTTGTAGTGGGAGCAAT
KRP1 (qRT)_R	TCTTCCTCTTCGTACCCCGTCG
KRP2 (qRT)_F	TCGTCGGTTTCGTGTTGTTCTACA
KRP2 (qRT)_R	GATCGTCACCGTTATTTTCCTCAA
KRP3 (qRT)_F	ACAGAGGCTATTCATGGAGAAGTACAAC
KRP3 (qRT)_R	ACCCATTCGTAACGTCCGCTG
KRP4 (qRT)_F	ACACACTCAAAGCTTCAACAGGAC
KRP4 (qRT)_R	AAGCTTTGTAGACGATCCCGG
KRP6 (qRT)_F	CACCAGCAATTTCAGAAAAGAGACG
KRP6 (qRT)_R	GGAGTCTTCCTCACCCCCGG
SIM (qRT)_F	GGCTGCACCACTCCCACTTCT
SIM (qRT)_R	ACGGTGTGGAAGGTGGACGG
SMR1 (qRT)_F	CGCCGTCGTAGACTCTCCACCT
SMR1 (qRT)_R	CATCAGAGCCGCCGTAGCCGA
CCS52A2 (qRT)_F	TGTGGTTACTGGTGTTAGCCCT
CCS52A2 (qRT)_R	GCCGGCGCATCCAATACCTTA

Supplemental Materials and Methods

Plant Work and Genetics

The *ucn-1* allele segregated in a Mendelian fashion (total plants scored: 136; wild type: 101, *ucn-1*: 35), as did the other *ucn* alleles (*ucn-7*: 62/18; *ucn-8*: 59/21; *ucn-9*: 62/18; *ucn-10*: 61/19). The TILLING-derived mutations in homozygous form were confirmed in M3 plants by sequencing. Mutant plants were outcrossed to Col *er-105*. The *ucn-1* and *ucn-10* mutants show the strongest phenotype with *ucn-9*, *ucn-8* and *ucn-7* exhibiting consecutively weaker phenotypes. T-DNA insertion lines were received from the SALK collection (6) and the Syngenta Arabidopsis Insertion Library (SAIL) (7) (*ucnl-1*, SAIL_238-A09, Col). The gene trap line GT931.DS5 (*ucnl-2*, L*er*) was obtained from the Cold Spring Harbor Lab Genetrap collection (http://genetrap.cshl.org) (8, 9). All lines were ordered through the Arabidopsis Biological Resource Center (ABRC, http://www.arabidopsis.org/abrc/index.jsp).

Map-Based Cloning of *UCN*

Using three separate Ler/Col F2 mapping populations *ucn-1* was initially genetically linked to a single region on the lower arm of chromosome 1 between markers CIW1 and F13011. Further fine-mapping placed *ucn-1* in a 129.2 kb interval between two self-generated CAPS markers in At1g51040 and At1g51380 (Fig. S3*A*). Two partially overlapping genomic BACs cover the interval. F23H24 and F11M15 span 45.3 kb and 105.8 kb, respectively, and share an 7.9 kb overlap. The two inserts were cloned in a binary-BAC vector (BIBAC2) (10) and constructs were transformed into *ucn-1* plants. Corresponding transgenic T1 *ucn-1* plants were scored for floral and ovule

phenotypes. Both constructs were able to rescue the *ucn-1* mutant phenotype. The result indicated that UCN resides on the 7.9 kb overlap region. This interval contains three annotated genes (Fig. S3*A*). To identify the *ucn-1* mutation we sequenced the 7.9 kb using genomic DNA from *ucn-1*, Ler and Col and found a single G to A transition at position 18958015 in *ucn-1* only. The mutation resides in the coding sequence of the predicted intronless At1g51170.

To generate At1g51150, At1g51160, and At1g51170 (*UCN*) genomic rescue constructs, genomic DNA of the three genes (Fig. S3*A*) was PCR amplified using L*er* genomic DNA as template and cloned into pCAMBIA2300. Only the construct harbouring 3.8 kb of At1g51170 genomic DNA (amplified with primers UCN (gen KpnI)_F/ UCN (gen PstI)_R) was able to rescue the mutant phenotype (> 100 T1 lines) (Fig. S3*D*).

Molecular Characterization of *UCNL*

Bioinformatic comparisons including the analysis of public cDNA-repositories suggest *UCNL* (At3g20830) to be intronless with a 1298 bp transcript with a 5' untranslated region of 10 bp, a coding sequence of 1227 bp and a 3' untranslated region of 61 bp. We analyzed by sequencing the insertion sites of five T-DNA lines within *UCNL* (Fig. S3*C*; Table S2).

Bioinformatic Analysis

Sequence searches were performed using the BLAST algorithm (11) and domain searches were done using the PFAM database (12).

Chlorophyll Fluorescence Measurements, In Vitro Transcription and Translation, Chloroplast Isolation and Protein Import

In vivo Chl a fluorescence of leaves was measured using the Pulse Amplitude Modulation 101/103 (Walz) as described (13). In vitro transcription translation of full-length cDNAs, chloroplast isolation and chloroplast import assays were done as described (14).

Protein Extraction and Immunoblotting

Rabbit polyclonal anti-UCN antibody was tested by immunoblotting using bacterially-expressed and affinity-purified recombinant proteins (GST:UCN, GST:UCN_{G165S}, GST:UCNL, BSA (as a non-specific control)). For the detection of endogenous UCN and UCNL proteins, total protein extracts were prepared in extraction buffer (50 mM Tris-HCl, pH 7.5, 150 mM NaCl, 0.5% Triton X-100, 10 μM MG132, 0.1 μM PMSF, and protease inhibitor cocktail [Sigma-Aldrich]) from roots of 12-day-old seedlings grown on MS medium supplemented with 1% sucrose. Root extracts were centrifuged for 5 min at 14,000g and the supernatant was mixed with 2× Laemmli loading buffer and heated at 95°C for 5 min prior to loading onto the gels. The anti-UCN antiserum and the preimmune serum were used at a dilution of

1:2000. Donkey anti-rabbit serum conjugated with peroxidase (1:5000) served as secondary antibody. Signals were detected using the SuperSignal West Femto Maximum sensitivity substrate (Thermoscientific, USA) and a luminescent image analyzer (LAS-4000 mini, Fujifilm, Germany). Loading controls were run on separate gels stained by Coomassie Brilliant Blue.

Confocal laser scanning microscopy

After excitation at 488 nm with a multi-line argon laser, GFP fluorescence was detected using 502-512 nm slit width. One-way scan images (scan rate 12.5 µs/pixel, 512x512 pixels, Kahlman frame, average of four scans) were obtained using an Olympus PLAPO 40x water objective. BiFC images were also acquired using a PLAPO 40x water objective. Excitation and emission wavelengths were as follows: YFP: 514 nm excitation, 527 nm emission; chlorophyll autofluorescence, 470 nm excitation, 680 nm emission; mCherry: 587 nm excitation, 610 nm emission. Images of immunolocalized UCN/UCNL in roots were taken using an UApo 40x oil objective. Excitation and emission wavelengths were as follows: Alexa Fluor™, 495 nm excitation, 519 nm emission; DAPI, 358 nm excitation, 461 nm emission.

Ovule Development: Double-Mutant Analysis.

The different mutants used in the double mutant analysis were described before: *ale2-1* (15); *acr4-2* (16); *ats-3* (17); *ant-72F5* and *bel1-1460* (18); *ino-2* (18, 19); *nzz-2* and *sub-1* (20, 21); *sup-5* (22). Double mutants were identified by direct phenotypic

inspection (plants showing an *ucn-1* floral phenotype and corresponding ovule aberrations) and occurred with expected frequencies for a Mendelian di-hybrid cross.

Supplemental References

1. Meister RJ, Kotow LM, Gasser CS (2002) *SUPERMAN* attenuates positive *INNER NO OUTER* autoregulation to maintain polar development of *Arabidopsis* ovule outer integuments. *Development* 129:4281–4289.

2. Menges M, de Jager SM, Gruissem W, Murray JA (2005) Global analysis of the core cell cycle regulators of Arabidopsis identifies novel genes, reveals multiple and highly specific profiles of expression and provides a coherent model for plant cell cycle control. *Plant J* 41:546–566.

3. Shih MC, Heinrich P, Goodmann HM (1991) Cloning and chromosomal mapping of nuclear genes encoding chloroplast and cytosolic glyceraldehyde-3-phosphate dehydrogenase from *Arabidopsis thaliana*. *Gene* 104:133–138.

4. Hoefle C et al. (2011) A barley ROP GTPase ACTIVATING PROTEIN associates with microtubules and regulates entry of the barley powdery mildew fungus into leaf epidermal cells. *Plant Cell* 23:2422–2439.

5. Truernit E et al. (2008) High-resolution whole-mount imaging of three-dimensional tissue organization and gene expression enables the study of phloem development and structure in *Arabidopsis*. *Plant Cell* 20:1494–1503.

6. Alonso JM et al. (2003) Genome-wide insertional mutagenesis of *Arabidopsis thaliana*. *Science* 301:653–657.

7. Sessions A et al. (2002) A high-throughput Arabidopsis reverse genetics system. *Plant Cell* 14:2985–2994.

8. Martienssen RA (1998) Functional genomics: probing plant gene function and expression with transposons. *Proc Natl Acad Sci U S A* 95:2021–2026.

9. Sundaresan V et al. (1995) Patterns of gene action in plant development revealed by enhancer trap and gene trap transposable elements. *Genes Dev* 9:1797–1810.

10. Hamilton CM (1997) A binary-BAC system for plant transformation with high-molecular-weight DNA. *Gene* 200:107–116.

11. Altschul SF, Gish W, Miller W, Myers EW, Lipman DJ (1990) Basic local alignment search tool. *J Mol Biol* 215:403–410.

12. Finn RD et al. (2008) The Pfam protein families database. *Nucleic Acids Res* 36:D281–8.

13. Varotto C et al. (2000) Disruption of the Arabidopsis photosystem I gene psaE1 affects photosynthesis and impairs growth. *Plant J* 22:115–124.

14. Armbruster U et al. (2009) Chloroplast proteins without cleavable transit peptides: rare exceptions or a major constituent of the chloroplast proteome? *Mol Plant* 2:1325–1335.

15. Tanaka H et al. (2007) Novel receptor-like kinase ALE2 controls shoot development by specifying epidermis in Arabidopsis. *Development* 134:1643–1652.

16. Gifford ML, Dean S, Ingram GC (2003) The *Arabidopsis ACR4* gene plays a role in cell layer organisation during ovule integument and sepal margin development. *Development* 130:4249–4258.

17. McAbee JM et al. (2006) *ABERRANT TESTA SHAPE* encodes a KANADI family member, linking polarity determination to separation and growth of Arabidopsis ovule integuments. *Plant J* 46:522–531.

18. Schneitz K, Hülskamp M, Kopczak SD, Pruitt RE (1997) Dissection of sexual organ ontogenesis: a genetic analysis of ovule development in *Arabidopsis thaliana*. *Development* 124:1367–1376.

19. Villanueva JM et al. (1999) *INNER NO OUTER* regulates abaxial/adaxial patterning in *Arabidopsis* ovules. *Genes Dev* 13:3160–3169.

20. Chevalier D et al. (2005) *STRUBBELIG* defines a receptor kinase-mediated signaling pathway regulating organ development in *Arabidopsis. Proc Natl Acad Sci U S A* 102:9074–9079.

21. Schiefthaler U et al. (1999) Molecular analysis of *NOZZLE*, a gene involved in pattern formation and early sporogenesis during sex organ development in *Arabidopsis thaliana. Proc Natl Acad Sci U S A* 96:11664–11669.

22. Gaiser JC, Robinson-Beers K, Gasser CS (1995) The Arabidopsis *SUPERMAN* gene mediates asymmetric growth of the outer integument of ovules. *Plant Cell* 7:333–345.